# Turbulence and Transport Suppression Scaling with Flow Shear on the Large Plasma Device

D.A. Schaffner,[1] T.A Carter,[1] G.D. Rossi,[1] D.S. Guice,[1] J.E. Maggs,[1] S. Vincena,[1] and B. Friedman[1]
*Department of Physics and Astronomy, University of California, Los Angeles*

(Dated: 15 December 2012)

Continuous control over azimuthal flow and shear in the edge of the Large Plasma Device (LAPD) [W. Gekelman, *et. al*, Rev. Sci. Instr. **62**, 2875 (1991)] has been achieved using a biasable limiter. This flow control has allowed a careful study of the effect of flow shear on pressure-gradient-driven turbulence and particle transport in LAPD. The combination of externally-controllable shear in a turbulent plasma along with the detailed spatial diagnostic capabilities on LAPD makes the experiment a useful testbed for validation of shear suppression models. Motivated by these models, power-law fits are made to the density and radial velocity fluctuation amplitudes, particle flux, density-potential crossphase and radial correlation length. The data show a break in the scaling these quantities with shearing at around a normalized shearing rate of one (shearing rate ($\gamma_s$) equal to the turbulent decorrelation rate ($1/\tau_{\rm ac}$). No one model captures the trends in the data across all values of shearing, but some models successfully match the trend in either the weak ($\gamma_s\tau_{\rm ac} < 1$) or strong shearing limits ($\gamma_s\tau_{\rm ac} > 1$).

## I. INTRODUCTION

Suppression of turbulence and turbulent transport by flow shear has been observed on a multitude of different magnetized plasma experiments[1–6]. While the importance of cross-field flow shear for the successful high confinement operation of fusion devices is well recognized[?] , we still lack a fully first-principles understanding of how sheared flow regulates turbulence and transport. The development of this understanding is essential in the development of a predictive capability for transport for current and future devices such as ITER. Experimental validation of shear suppression models is a critical part of this development process, providing motivation for experiments in which the response of turbulence to shear flow is carefully documented. External control of flow shear in a magnetized plasma has been previously achieved in a number of torodial devices using biased electrodes to drive cross-field currents and provide torque to drive plasma rotation[8,9]. Transport reduction and confinement transitions have been observed in response to biasing and this response has been compared to models for shear suppression, in particular in work from TEXTOR group[10–12].

Biasing has been used to induce rotation and transitions in particle confinement in the Large Plasma Device (LAPD)[? ?] . Recently, a new data set has been gathered on LAPD in which the flow shear was continuously varied using a new biasable limiter[6]. These experiments demonstrated the shear suppression in measurements of a number of turbulent quantities including cross-field particle flux, density and radial $E \times B$ velocity fluctuations, density-velocity crossphase, and radial correlation length. Moreover, the scan included data points in both the weak and strong shearing regime, as defined by the ratio of shearing rate to inverse autocorrelation time. This provides the ability for comparison to models which make separate predictions for each regime.

!!HERE YOU SHOULD GO AHEAD AND CITE ALL OF THE MODELS YOU WILL USE LATER!!

Models based on radial decorrelation of turbulent structures by sheared flow are prevalent in the theoretical literature and provide a number of predictions concerning the quantitative scaling of turbulent quantities with shear[3]. The basic premise underlying these models is the competition between linear or nonlinear turbulence dynamics and the tendency of sheared flows to "rip apart" or decorrelate turbulent structures; leading to the potential of reduced fluctuation amplitude and decreased radial transport step-size. A large number of theoretical models have been developed which use this underlying principle. Variation in the predictions of these models arise from assumptions: strength of flow shear compared to turbulence timescales (strong vs weak), the underlying instability driving the turbulence (i.e. Ion Temperature Gradient (ITG) or Resistive Ballooning), as well as consideration of passive versus dynamic scalars.

This paper presents experimental fits of density fluctuation amplitude, radial velocity fluctuation amplitude, particle flux, crossphase, diffusivity and radial correlation length as functions of flow shear and compares them to a number of model predictions. No one model predicts how all the quantities scale though some models do make favorable comparisons for some quantities, but unfavorable comparisons to others. The fits generally show a stronger decrease in turbulent fluctuations than crossphase as a contributer to reduction of particle flux. Fits to the suppression of measured radial diffusion—which incorporates the changes in density gradient—compare well to numerical simulation predictions. The ability to make favorable predictions for some quantities while not other perhaps suggests a dependence on turbulent conditions for determining shear suppression and call for specific calculations for LAPD plasmas to be made.

This paper is organized as follows. A brief review of shear decorrelation models is provided in Section II, followed by a discussion of the LAPD experiments in Section III. In Section IV, the approach for model fitting

of the experimental data is discussed and the results of these fits are presented in Section V. Finally a discussion of how these fits compare to analytic and simulation model predictions is given in Section VI.

## II. MODELS OF SHEAR SUPPRESSION

Two of the earliest models of shear suppression were decorrelation models developed by Biglari, Diamond, Terry[16] (hereafter BDT) and Shaing[17]. The BDT theory presents a generalized analysis of the transport of a passive scalar in a mean sheared flow in the strong-shear regime with constant turbulent drive (pressure gradient). The BDT model predicts that normalized fluctuation amplitude scales directly with shear to the -2/3 power:

$$\frac{\langle|\tilde{\xi}|^2\rangle}{\langle|\tilde{\xi}|^2\rangle_{\gamma_s=0}} \sim (\gamma_s\tau_{ac})^{-2/3} \tag{1}$$

where $\eta$ can be any quantity such as density or temperature. Conversely, the Shaing model focuses on the weak shearing limit and predicts a scaling of the form:

$$\frac{\langle|\tilde{\xi}|^2\rangle}{\langle|\tilde{\xi}|^2\rangle_{\gamma_s=0}} \sim 1-\alpha(\gamma_s\tau_{ac})^2 \tag{2}$$

Where $\alpha$ is a constant containing mode number information.

Zhang and Mahajan[18,19] developed a model which included the self-consistent modification of the fluctuation spectrum and the diffusion coefficient by flow shear. This allowed the development of a model which could span both the weak and strong shear regimes which for weak turbulence can be represented as,

$$\left(\frac{\langle|\tilde{\xi}|^2\rangle}{\langle|\tilde{\xi}|^2\rangle_{\gamma_s=0}}\right)^{-1} \sim 1+\alpha(\gamma_s\tau_{ac})^2 \tag{3}$$

The resulting model shows correspondence to the Shaing model in the weak shearing regime while the BDT model can be recovered in the strong shearing regime but only for the case where the diffusion coefficient is constant (independent of fluctuation amplitude). Furthermore, they extend the model to incorporate the effect of changes in turbulent drive (gradient scale-length), showing that shear suppression of fluctuation amplitude is enhanced by a steeper equilibrium gradient.

Work by Ware and Terry[20,21] made predictions for the effect of shearing on particle transport specifically in resistive pressure-gradient driven turbulence. Their work predicted a decrease in flux as $\Gamma_p \sim 1-\gamma_s^2$ in the weak shear limit. Additionally, the model predicted a decrease in the cosine of the crossphase between density and radial velocity fluctuations of the form $1-\omega_s^2$. They too incorporated the modification of the pressure gradient, formulating an expression for shearing suppression of radial particle diffusivity of the form:

$$\frac{D}{D(\gamma_s=0)} \sim 1-\beta(\gamma_s)^2 \tag{4}$$

where $\beta$ is a constant which depends on the linear growth rate and radial mode width.

Further work by Terry, Newman and Ware[22] examined the modification of flux in the strong shearing regime for a non-mode-specific turbulent system, predicting a direct scaling of $\Gamma_p \sim \gamma_s^{-4}$ overall. Here fluctuation amplitude reduction contributing one power while crossphase reduction contributed three powers of $\gamma_s$, indicating that, in the strong shearing limit, crossphase modification is the dominant flux suppression mechanism rather than reducation of the fluctuation amplitude.

Kim and Diamond[23] recast the decorrelation model to include resonance absorption between the shear flow and fluctuations leading to a much weaker dependence of particle flux on shear, $\Gamma_p \sim \gamma_s^{-1}$, and even weaker dependence of the crossphase on shear: $\cos(\theta_{nv_r}) \sim \gamma_s^{-1/6}$. In the model fluctuations decreased as $|\tilde{n}|^2 \sim \gamma_s^{-5/3}$. Additional work along these lines[24] considered a more self-consistent model for the turbulence, treating the fluctuating flows dynamically using interchange drive. This model predicted a decrease in fluctuating radial velocity amplitude as a function of shear which scales as $|\tilde{v_r}|^2 \sim \gamma_s^{-3}$ in the weak shear limit, and as $|\tilde{v_r}|^2 \sim \gamma_s^{-4}$ in the strong-shearing limit.

Most recently, Leconte et al.[25] found different scalings for flux, fluctuations and crossphase in the strong shear regime depending on relative shearing strength relative to a characteristic time and shearing spatial gradient relative to the inhomogeneity gradient. Work by Newton and Kim has utilized numerical simulations to determine shearing scalings in a generic model[26,27].

!!Again, why mention this if you don't show the scalings and don't compare?

## III. SHEAR SUPPRESSION EXPERIMENTS

The Large Plasma Device[28] (LAPD) is a 17m long, ∼60cm diameter cylindrical plasma produced by a barium-oxide coated nickel cathode. In the experiments reported here, a plasma of density $\sim 2\times10^{12}$ cm$^{-3}$ and peak temperature of 8eV is produced in a uniform solenoidal magnetic field of 1000G. All measurements reported here were collecting using Langmuir probes recording floating potential, $V_f$, or ion saturation current, $I_{\rm sat}$. Azimuthal electric field fluctuations, $\tilde{E}_\theta$, are found by taking the simultaneous difference in two $V_f$ signals separated a small azimuthal distance apart. Turbulent particle flux $\Gamma \propto \left\langle \tilde{n}_e\tilde{E}_\theta \right\rangle$ is determined through correlating density fluctuations with $\tilde{E}_\theta$ where it assumed that $E_\theta$ produces radial $E\times B$ flow. The relative crossphase

between fluctuation time-series is determined through the cross-spectrum of the quantities. That is,

$$\theta = \tan^{-1} \frac{\langle Q(f,r)\rangle_{f,r}}{\langle C(f,r)\rangle_{f,r}} \quad (5)$$

where Q and C are the imaginary and real parts of the cross-spectrum, calculated from product of the complex FFTs of the two time-series in question as in,

$$G(f,r) = \hat{x}^*(f,r)\hat{y}(f,r) \quad (6)$$

where the cross-spectrum is first averaged over frequencies to power-weight the crossphase signal, and then averaged radially, before the phase is determined. Finally, steady-state azimuthal flow, $V_\theta$ is determined through the radial derivative of plasma potential profiles measured using a swept-Langmuir probe technique again assuming only $E \times B$ flow. The shearing rate is computed as $\gamma_s = d/dr(V_\theta)$.

A large annular aluminum limiter was installed in LAPD to provide a parallel boundary condition for the edge plasma and is biased relative to the cathode of the plasma source to control plasma potential and cross-field flow. A diagram of the limiter arrangement and biasing circuit is shown in Fig. 1.

A recent experiment on the LAPD demonstrated the ability to achieve continuous control of steady-state azimuthal flow and flow shear through the use of these biasable limiters[6]. Spontaneous rotation is observed in LAPD in the ion diamagnetic direction. This spontaneous flow can be reduced and reversed into the electron diamagnetic direction as the limiter bias is increased. This results in a continuous variation of edge flow and flow shear including zero flow and flow shear states. Shearing rates are acheived up to about five times the turbulent inverse autocorrelation time $\tau_{ac}^{-1}$ as measured in the unsheared state. Radial particle flux and fluctuation amplitude are reduced as shearing rate is increased and the resulting transport changes cause observable steepening of the density gradient. Figure 2 shows the experimental results for measurements of density fluctuation amplitude, radial velocity amplitude and density-radial velocity crossphase as functions of normalized shearing rates. The shearing rates achieved span two regimes: a weak-shear regime where $\gamma_s\tau_{ac} < 1$ and a strong-shear regime where $\gamma_s\tau_{ac} > 1$. The blue solid lines correspond to the best fits for the strong-shear cases while the green are the best fits for the weak-shear case. Similar plots for particle flux and diffusivity $D = \Gamma/|\nabla n|$ are shown in Fig. 3. Error bars of +/-20% for each quanitity are shown on the plots and used in the fits, reflecting a statistical error from the number of shots used to average the quanity ($\sigma \sim 1/\sqrt{nshots}$).

Measurements of the radial correlation length were recorded as a function of shearing rate (applied bias) using a two-probe correlation technique. A reference probe collecting $I_{cmrsat}$ is kept stationary at a particular axial and radial location within LAPD. A second

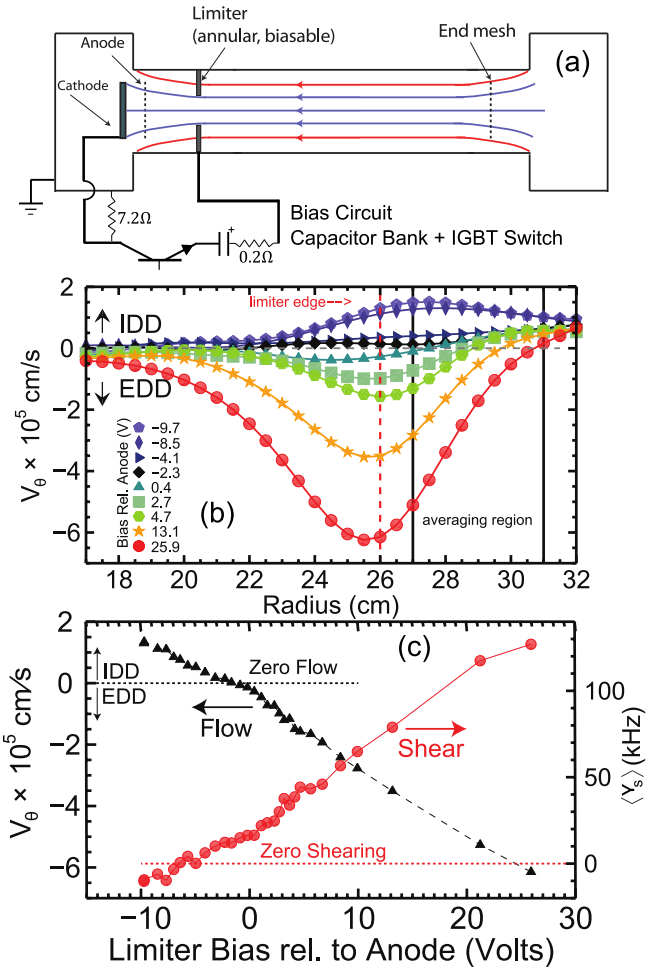


FIG. 1. (a) Diagram of the LAPD device showing relative location of the annular limiter and basic biasing setup. (b) Velocity profiles using plasma potential from swept measurements. (c) Flow at the limiter edge (black, triangles) and mean shearing rate, averaged over $27 < r < 31$cm (red, circles).

Langmuir probe situated at an axial point closer to the cathode is moved shot-to-shot in a rectangular grid around the radial location of the reference probe. The cross-field cross-correlation function of these two measurements is computed shot-to-shot for a delay time $\tau$ as $C(x,y,\tau) = \langle I_{ref}(x,y,t) I_{mot}(x,y,t+\tau)\rangle$. Fig. 4(a) shows the normalized correlation function $C(x,y)/C_{max}$ for the unbiased state (flow in the IDD), a minimum shear state, and a high bias state (large EDD flow) with a reference probe located at $x = 29.5$cm, $y = 0$cm (right in the middle of the shear layer). The black curve represents the contour line where $C(x,y)/C_{max} = 0.5$. The radial correlation length $\Delta r_c$ is defined here as the radial width of this black curve through the reference probe location. The variation of the correlation length versus shearing rate is shown in Fig. 4 (normalized to the maximum radial correlation length calculated for all biases). The correlation length is found to decrease substantially with shearing. A break in the trend of decreasing correlation length is observed for larger shearing rates where

the correlation function appears to be dominated by a coherent mode (which also appears in the temporal power spectrum).

Some acheived parameters regimes for the shearing rat and density gradient length scales are presented in Fig. 5. The shearing scale length is calculated as in $L_\gamma = |\nabla \ln(v_{E\times B}|^{-1}$. This value is compared to the density gradient scale length, $L_n = |\nabla \ln n|^{-1}$ for each bias and mapped to a normalized shearing value. This plot shows that for the all of the strong shearing regime, and nearly half of the weak shearing regime, $L_n > L_\gamma$. The reverse is true only for the weakest shearing points. This quantity $L_\gamma/L_n$ can be utilized in asymptotic limits similar to the $\gamma_s/\tau_{ac}^{-1}$ ratio for models[25].

## IV. EXPERIMENTAL SHEAR SUPPRESSION SCALING

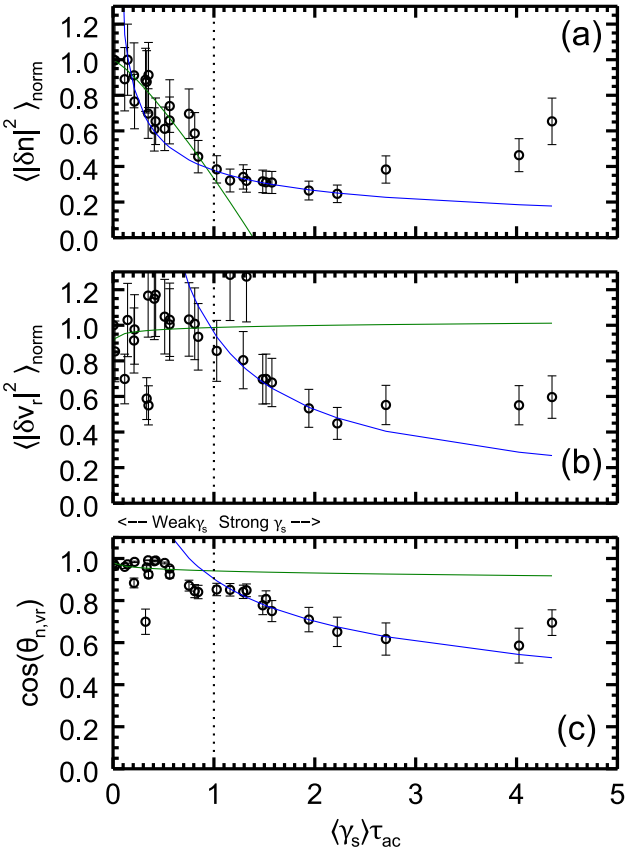


FIG. 2. Scaling of (a)density fluctuation amplitude, (b)radial velocity fluctuation amplitude, and (c)relative crossphase between density and radial velocity fluctuations. Density and velocity fluctuation are each normalized to the value measured at minimum shear. The green curves correspond to $1-\gamma_s^\nu$ fits of the weak shear regime. The blue curves correspond to $\gamma_s^\nu$ fits.

The variation of the experimentally measured quantities with normalized shearing rate was fit to functions motivated by models discussed above: functions of the

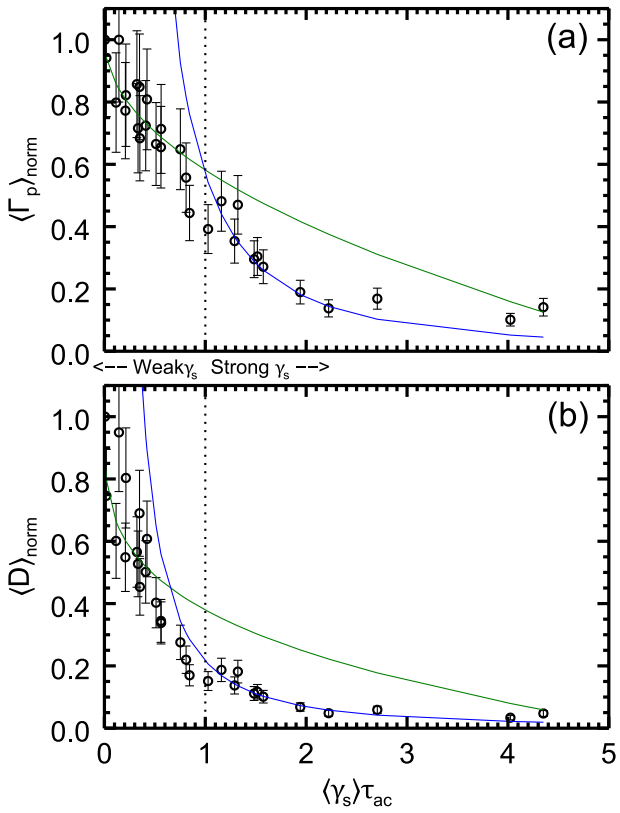


FIG. 3. Scaling of (a)radial particle flux and (b)diffusion coefficient each normalized to the value at minimum shear, $\Gamma_p^0 = 1.7\times10^{16} cm^{-2}$ and $D_0 = 36.7 m^2/s$. The green curves correspond to $1-\gamma_s^\nu$ fits of the weak shear regime with $\nu = 0.501$ for flux and $\nu = 0.418$ for D. The blue curves correspond to $\gamma_s^\nu$ fits with $\nu = -1.719$ for flux and $\nu = -1.646$ for D.

TABLE I. Power-law fits for $|\tilde{n}^2|$ with shear for frequencies in 350Hz to 100kHz. Model form refers to how the shearing relates to the quantity in question, with C a constant and $\nu$ the power exponent.

| Model form | $\gamma_s$ regime | $\nu$ | $\chi^2$ | $\chi^2/ndf$ |
|---|---|---|---|---|
| $\sim 1-C\gamma_s^\nu$ | $\gamma_s\tau_{ac}<1$ | 1.228 | 1.091 | 0.0642 |
| $\sim 1-C\gamma_s^\nu$ | $\gamma_s\tau_{ac}>1$ | 0.231 | 0.0332 | 0.0037 |
| $\sim C\gamma_s^\nu$ | $\gamma_s\tau_{ac}<1$ | -0.116 | 0.1791 | 0.0094 |
| $\sim C\gamma_s^\nu$ | $\gamma_s\tau_{ac}>1$ | -0.512 | 0.0024 | 0.0003 |

TABLE II. Power-law fits for $|\tilde{v}_r^2|$ scaling with shear for frequencies in 350Hz to 100kHz. Model form refers to how the shearing relates to the quantity in question, with C a constant and $\nu$ the power exponent.

| Model form | $\gamma_s$ regime | $\nu$ | $\chi^2$ | $\chi^2/ndf$ |
|---|---|---|---|---|
| $\sim C\gamma_s^\nu$ | $\gamma_s\tau_{ac}<1$ | 0.016 | 0.2121 | 0.0117 |
| $\sim C\gamma_s^\nu$ | $\gamma_s\tau_{ac}>1$ | -0.866 | 0.0037 | 0.0005 |

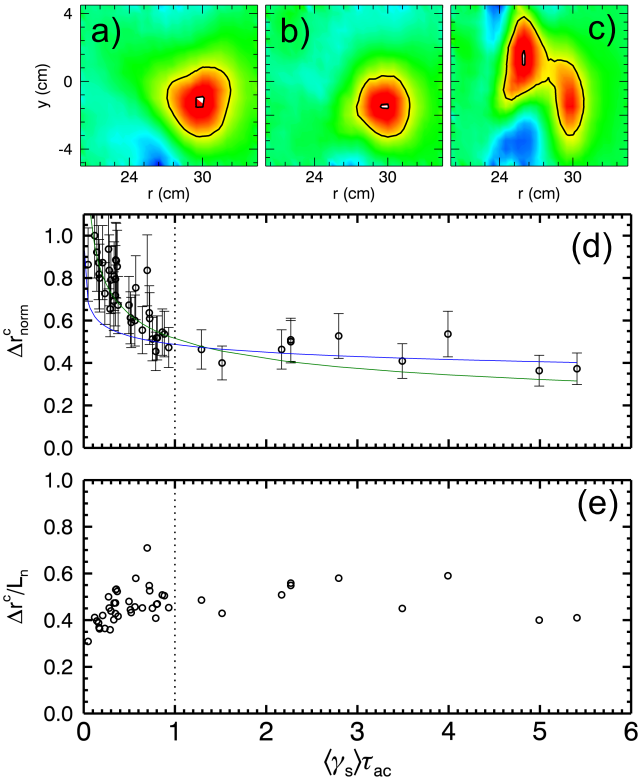


FIG. 4. Normalized correlation functions for (a)unbiased state, (b)no shear state, and (c)high bias, high EDD flow state where the black curve represents a decrease of 0.5 from peak. (d)Radial correlation length normalized to maximum correlation length versus normalized shearing rate. (e)Ratio of radial correlation length to density gradient scale length.

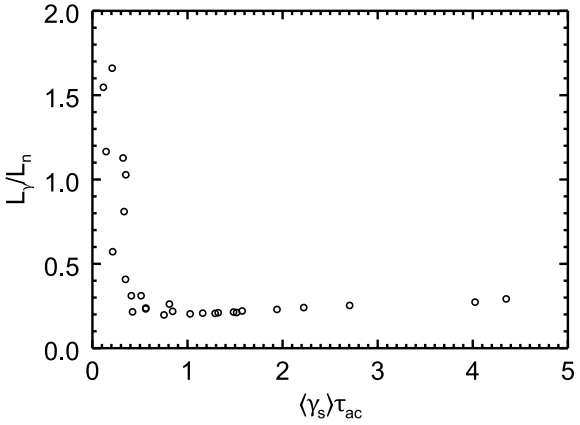


FIG. 5. Ratio of shearing length scale to density gradient length scale versus normalized shearing in the radial region of 27 to 31cm.

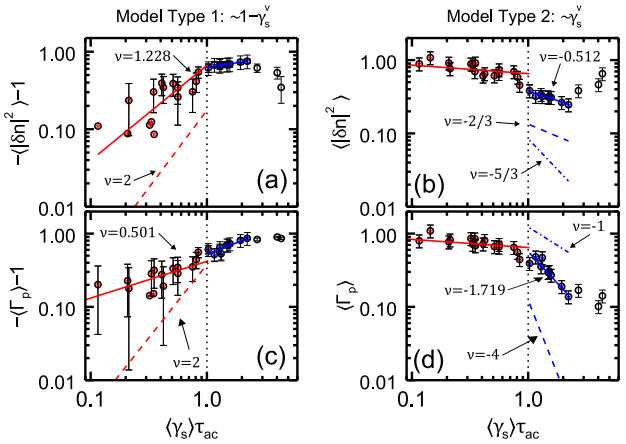


FIG. 6. Log-Log plot of (a-b)density fluctuation amplitude and (c-d)particle flux versus shearing. Weak shearing fits, (a) and (c), are shown with the solid red lines and a theoretical prediction—dashed line—of $\nu = 2$ is included for comparison of slope (line is manually offset). Strong shearing fits, (b) and (d), are shown with the solid blue lines and theoretical predictions are indicated with the dashed lines.

TABLE III. Power-law fits for $\Gamma_p$ scaling with shear for frequencies in 350Hz to 100kHz. Model form refers to how the shearing relates to the quantity in question, with C a constant and $\nu$ the power exponent.

| Model form | $\gamma_s$ regime | $\nu$ | $\chi^2$ | $\chi^2/ndf$ |
|---|---|---|---|---|
| $\sim 1 - C\gamma_s^\nu$ | $\gamma_s\tau_{ac} < 1$ | 0.501 | 0.332 | 0.0189 |
| $\sim 1 - C\gamma_s^\nu$ | $\gamma_s\tau_{ac} > 1$ | 0.638 | 0.923 | 0.103 |
| $\sim C\gamma_s^\nu$ | $\gamma_s\tau_{ac} < 1$ | -0.111 | 0.146 | 0.0077 |
| $\sim C\gamma_s^\nu$ | $\gamma_s\tau_{ac} > 1$ | -1.719 | 6.54 | 0.726 |

TABLE IV. Power-law fits for $cos(\theta_{nv_r})$ scaling with shear for frequencies in 350Hz to 100kHz. Model form refers to how the shearing relates to the quantity in question, with C a constant and $\nu$ the power exponent.

| Model form | $\gamma_s$ regime | $\nu$ | $\chi^2$ | $\chi^2/ndf$ |
|---|---|---|---|---|
| $\sim 1 - C\gamma_s^\nu$ | $\gamma_s\tau_{ac} < 1$ | 0.226 | 6.1140 | 0.3320 |
| $\sim C\gamma_s^\nu$ | $\gamma_s\tau_{ac} < 1$ | -0.020 | 0.0369 | 0.0019 |
| $\sim C\gamma_s^\nu$ | $\gamma_s\tau_{ac} > 1$ | -0.365 | 0.0023 | 0.0003 |

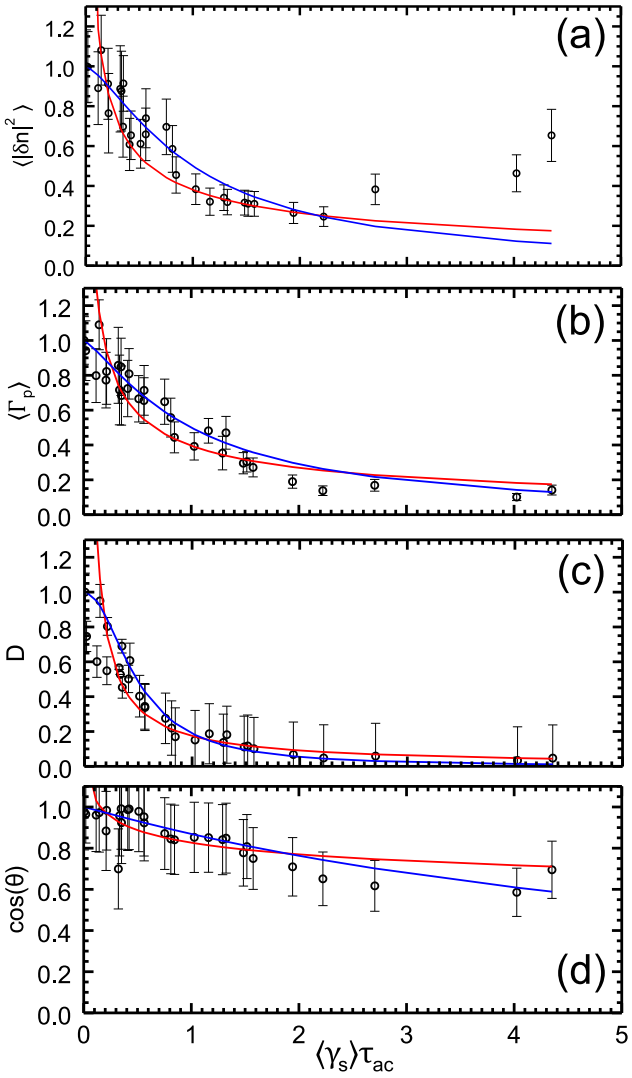


FIG. 7. Fits over a shearing range spanning both weak and strong regimes for (a) density fluctuation amplitude, (b)particle flux, (c)Diffusivity, and (d)Crossphase. Red lines correspond to $\sim C\gamma_s^\nu$ model while the blue curves correspond to the $\sim 1/(1+C\gamma_s^\nu)$ model.

form $1-\gamma_s^\nu$ (hereafter M1 or model type 1) and of $\gamma_s^\nu$ (hereafter M2). For M1, the measured quantity, $y$, was normalized to the value at zero shear, then transformed as $-(1-y)$. Then, taking the logarithm of both sides, a linear fit was made for points in the weak shear and in the strong shear separately. The resulting slope of the fit is taken as the power $\nu$. For M2, no transformation of the quanitity $y$ to $-(1-y)$ is made before taking the logarithm and fitting. For a complete comparison to the wide range of model predictions made, fits were made for density fluctuation amplitude, radial particle flux, density-radial velocity fluctuation crossphase, radial velocity (ExB) fluctuation amplitude, radial correlation length, and experimentally determined diffusivity ($\Gamma/|\nabla n|$). The best fits are summarized in Table I- VI for each model type and for both weak and strong shearing. The $\chi^2$ and $\chi^2$/ndf (where ndf is the number of degrees of freedom) is also indicated in the tables. For weak shear fits, all points less than the weak shear cutoff $\gamma_s\tau_{ac}$¡1 are used in the fit. For strong shear, all but the last three points are used. The last points appear to be strongly influenced by the presence of a coherent mode that develops in the highest shear and flow cases and is thought to be a break from the scaling observed in the strong shear regime. For quantities determined by averaging over frequency (e.g. density and velocity fluctuation amplitudes, flux and diffusivity) the frequency band used was 350Hz to 100kHz.

The log-log plots highlight the break in trend between weak and strong shear. It should be noted that in addition to turbulent quantities showing a different trend with shear below and above a normalized shearing rate of unity, at the same time, the density gradient scale length also shows a marked change in behavior[6], with a strong decrease of the gradient scale length in the weak shearing regime followed by saturation in the strong shear regime. Therefore care has to be taken in interpreting the change in the trends plotted above: it could be occurring due to a change in the shearing regime but also could be due to the change in trend for the turbulence drive.

Lastly, fits were made for shearing regions that spanned portions of both the weak and strong shearing regimes; specifically, a range that included all but the first two lowest shearing values and the three high shearing values—again, dropping the last three to avoid any influence of the coherent mode. The models used are M2 and a third model based on the Zhang and Mahajan interpolated form 3 which was designed to describe both weak and shear scaling (hereafter M3). Fits and $\chi^2$ values are displayed for density fluctuation amplitude, particle flux, diffusivity, and crossphase in Table VII and are shown plotted against the data in Figure 7.

TABLE V. Power-law fits for $D = \Gamma_p/\nabla n$ scaling with shear for frequencies in 350Hz to 100kHz. Model form refers to how the shearing relates to the quantity in question, with C a constant and $\nu$ the power exponent.

| Model form | $\gamma_s$ regime | $\nu$ | $\chi^2$ | $\chi^2/ndf$ |
|---|---|---|---|---|
| $\sim 1 - C\gamma_s^\nu$ | $\gamma_s\tau_{ac} < 1$ | 0.418 | 1.4710 | 0.0817 |
| $\sim 1 - C\gamma_s^\nu$ | $\gamma_s\tau_{ac} > 1$ | 0.197 | 0.0016 | 0.0002 |
| $\sim C\gamma_s^\nu$ | $\gamma_s\tau_{ac} < 1$ | -0.217 | 0.4200 | 0.0221 |
| $\sim C\gamma_s^\nu$ | $\gamma_s\tau_{ac} > 1$ | -1.646 | 0.0187 | 0.0021 |

TABLE VI. Power-law fits for $\Delta r_c$ scaling with shear for frequencies in 350Hz to 100kHz. Model form refers to how the shearing relates to the quantity in question, with C a constant and $\nu$ the power exponent.

| Model form | $\gamma_s$ regime | $\nu$ | $\chi^2$ | $\chi^2/ndf$ |
|---|---|---|---|---|
| $\sim C\gamma_s^\nu$ | $\gamma_s\tau_{ac} < 1$ | -0.290 | 5.8730 | 0.1630 |
| $\sim C\gamma_s^\nu$ | $\gamma_s\tau_{ac} > 1$ | -0.113 | 3.7040 | 0.3370 |

## V. RESULTS

### A. Density and Velocity Fluctuations

The best fits for scaling of density fluctuation amplitude are shown in Table I. For the weak shear regime, the $\chi^2$ values suggest M2 to be a slightly better fit to the data than M1. Though M1 is not used for prediction of strong shear scaling in the literature, a fit was made to it here for completeness; still, as with the weak shearing regime, values of $\chi^2$ show M2 to be a better model for the strong shearing regime as well.

The $\nu = -0.512$ fit for M2 in the strong shearing limit is reasonably close to the BDT prediction of $-(2/3)$. However, it should be reiterated that BDT assumes a fixed turbulence drive and that in this dataset, the gradient scale length decreases substantially as shearing is increased, resulting in an increase in turbulent drive. This actually implies a stronger than BDT scaling of fluctuation amplitude suppression overall. For weak shearing and M2, the experimental fit of $\nu = -0.116$ also suggests weaker scaling than the prediction by Kim and Diamond of $-(2/3)$.

TABLE VII. Power law fits for all quantities over a range that spans both weak and strong shearing. The smallest two shearing points are excluded to improve the fitting routine and the three highest shearing point are excluded to avoid effects of the coherent mode.

| Parameter | Model form | $\nu$ | $\chi^2$ | $\chi^2/ndf$ |
|---|---|---|---|---|
| $\langle\|\tilde{n}^2\|\rangle$ | $\sim 1/(1 + C\gamma_s^\nu)$ | 1.339 | 0.9435 | 0.0393 |
| $\langle\|\tilde{n}^2\|\rangle$ | $\sim C\gamma_s^\nu$ | -0.527 | 0.1280 | 0.0053 |
| $\langle\Gamma_p\rangle$ | $\sim 1/(1 + C\gamma_s^\nu)$ | 1.199 | 0.7899 | 0.0329 |
| $\langle\Gamma_p\rangle$ | $\sim C\gamma_s^\nu$ | -0.557 | 0.2691 | 0.0112 |
| $\langle D\rangle$ | $\sim 1/(1 + C\gamma_s^\nu)$ | 1.387 | 0.7375 | 0.0307 |
| $\langle D\rangle$ | $\sim C\gamma_s^\nu$ | -0.938 | 0.3490 | 0.0145 |
| $cos(\theta_{nv_r})$ | $\sim 1/(1 + C\gamma_s^\nu)$ | 1.043 | 3.8300 | 0.1596 |
| $cos(\theta_{nv_r})$ | $\sim C\gamma_s^\nu$ | -0.102 | 0.0340 | 0.0014 |

A prediction for the scaling of radial velocity fluctuation amplitude is only made by Kim and Diamond[24] in the dynamically evolved case. Fits, listed in Table II, suggest a much weaker scaling than predicted for both weak and strong shear. The weak shear fit actually shows a slight increase in fluctuation amplitude rather than a $\nu = -3$ scaling while in the strong shear regime a fit of $\nu = -0.866 << -4$ is found.

For the full shearing range, M2 appears to be a slightly better model than M3. The M2 fit is similar to the strong shear only fit, but clearly has a worse $\chi^2$ value.

### B. Flux and Diffusivity

Particle flux and diffusivity fits and $\chi^2$ results are show in in Table III and V respectively. Like density fluctuations, M2 seems to be slightly better than M1 for fitting data in the weak shear limit based on $\chi^2$ values. However, for strong shear, the M1 model actually has a much better fit then the M2 model, though M1 is not derived in the strong shearing limit in the literature. Despite the higher $\chi^2$, the fit of $\nu = -1.719$ falls in between the extremes of predictions of $\nu = -1$ and $\nu = -4$. The weak shear fit of $\nu = -0.111$ falls far short of the Kim and Diamond M2 prediction of $\nu = -2$. In addition to being the less well-fitted model, the predicted exponent for M1 in the weak shearing limit is also far less than the Terry and Ware value of $\nu = 2$.

Diffusivity, like flux, has lower $\chi^2$ values for M2 with weak shearing and for M1 with strong shearing. The only predictions for $D$ come from Terry and Ware with a functional form like M1 and a numerical simulation result from Newton and Kim[27] for evolved turbulence with a finite correlation time. The experimental fit of $\nu = 0.418$ again falls short of the predicted $\nu = 2$, though the M2 fit in the strong shearing limit with $\nu = -1.646$ is fairly close to the predicted value of $\nu = -1.75$.

### C. Crossphase and Correlation Length

Fits for the scaling of cosine of the crossphase between density and radial velocity fluctuations is shown in Table IV. M2 is found to fit better than M1 for both weak and strong shearing limits. The M2 fit in the weak limit of $\nu = -0.02$ and M2 fit in the strong limit of $\nu = -0.365$ both tend to support the prediction of mild scaling with crossphase made by Kim and Diamond [23,24] with $\nu = -(1/6)$ rather then the large scaling of $\nu = -3$ made by Terry[22]. It should be pointed out that the variation of cross-phase with shearing in this dataset is markedly different than what was observed in an earlier LAPD experiment where flow was driven by biasing the vacuum chamber wall[?] . This previous experiment was performed at lower magnetic field and at larger bias, resulting in a stronger $E \times B$ rotation and much stronger normalized shearing ($\gamma_s\tau$ac $\sim 20$). There

a strong modification of cross-phase was observed (with little to no amplitude reduction).

Finally, a fit to radial correlation length is made and compared to the prediction made by BDT[16]. Neither the weak shear fit of $\nu = -0.290$ nor the strong shear of $\nu = -0.113$ is unreasonably far from the predicted value of $\nu = -1/3$ though the $\chi^2$ values do not suggest a great fit to either model. It should again be noted that these correlation lengths are measured in the steady-state period when the density gradient scale length will have already adjusted due to the change in transport. Thus, this decrease in radial correlation length could be due to the turbulence adjusting to the new gradient scale length rather than a direct response to shearing. In Figure 4(b) the ratio of the radial correlation length to the density gradient scale length is shown, indicating that this ratio remains constant with shearing. In order to evaluate the effect of shearing on radial correlation length independent of changes to the gradient scale length, the correlation length could be studied in the transient phase after the flow is turned on but before the profile has had time to steepen. Investigation of the dynamics of this transition will be the subject of future work.

## VI. DISCUSSION

While the large variation in fits for six turbulent quantities makes careful model validation difficult, there are a number of conclusions that can be drawn from the analysis reported here. First the experimental results from this dataset show a distinct difference in scaling between the weak and strong shear regimes, consistent with expectations from many models. Second, models that predict scaling of turbulent quantities as $\gamma_s^\nu$ in general better fit the data (based on $\chi^2$ values) than models of the the form $1 - \gamma_s^\nu$ with an exception noted in the case of flux and diffusivity. Third, the data clearly supports the prediction that density fluctuation amplitude is more strongly suppressed than the crossphase and thus makes a more significant contribution to the suppression of radial transport. However it should be noted that at much stronger shearing (in previous LAPD datasets), dominant modification of crossphase is observed. Finally, as indicated by the wide range of predictions, the scaling of shear suppression may be dependent on the nature of the turbulence used in the model. Many of the suppression models discussed are mode specific such as resistive-drift turbulence for the Terry, Ware models or interchange for the later Kim, Diamond models. Neither of these two models fit the LAPD results quantitatively well which may suggest the need for a model based on LAPD-specific turbulent drive.

## VII. CONCLUSIONS

The results of this paper present power-law fits of experimental measurements of density fluctuations, radial velocity fluctuations, particle flux, crossphase, diffusivity and radial correlation length as a function of both weak and strong shearing as found on the LAPD. These results are compared to the myriad of models for prediction of shear suppression which are based on the physical idea of shear decorrelation of turbulent eddies. While some of the model predictions approach the experimentally measured values, most are only capable of being close to only one or two of the predicted quantities while generally far off on others. In the process of developing these analytic shear suppression models, assumptions must often be made about the type of turbulence involved (such as pressure-gradient driven turbulence versus rotational interchange driven turbulence) when it is likely, rather, that many types of free-energy are available in the actual experimental plasma (as on the LAPD where both drift waves and rotational interchange modes may be present). Simulation work which can incorporate more complex turbulent environments, then, could in this vein have some promise for better matching to experiment as well as analytical endeavors to develop a shear suppression model specifically for LAPD plasma. Lastly, there is, of course, the possibility that decorrelation models are not the correct models for predicting shear suppression. Comparison of this dataset to predictions made by alternative shear suppression models, such as suppression by shifted radial wavenumbers[?] , will be made in future work.


[1] K. Burrell, Phys. Plasmas **4**, 1499 (1997).
[2] K. Burrell, Phys. Plasmas **6**, 4418 (1999).
[3] P. Terry, Rev. Mod. Phys. **72**, 109 (2000).
[4] G. Van Oost , J. Adamek and V. Antoni, P. Balan, J.A. Boedo, P. Devynck, I. Duran, L. Eliseev, J.P. Gunn, M. Hron, C. Ionita, S. Jachmich, G.S. Kirnev, E. Martines, A. Melnikov, R. Schrittwieser, C. Silva, J. Stockel, M. Tendler, C. Varandas, M. Van Schoor, V. Vershkov and R.R. Weynants, Plas. Phys. Control Fusion **48**, 621 (2003).
[5] O. Sakai, Y. Yasaka and R. Itatani, Phys. Rev. Lett. **70**, 4071 (1993).
[6] D.A. Schaffner, T.A. Carter, G.D. Rossi, D.S. Guice, J.E. Maggs, S.Vincena and B. Friedman, Phys. Rev. Lett. **109**, 135002 (2012).
[7] K.H. Burrell, T.N. Carlstrom, E.J. Doyle, D. Finkenthal, P. Gohil, R.J. Groebner, D.L. Hillis, J. Kim, H. Matsumoto, R.A. Moyer, T.H. Osborne, C.L. Rettig, W.A. Peebles, T.L. Rhodes, H. St.John, R.D. Stambaugh, M.R. Wade and J.G. Watkins, Plas. Phys. Control Fusion **34**, 1859 (1992).
[8] R.J. Taylor, M.L. Brown, B.D. Fried, H. Grote, J.R. Liberati, G.J. Morales, P. Pribyl, D. Darrow and M. Ono, Phys. Rev. Lett. **63**, 2365 (1989).
[9] R.R. Weynants, G. Van Oost, G. Bertschinger, J. Boedo, P. Brys, T. Delvigne, K.H. Dippel, F. Durodie, H. Euringer, K.H. Finken, D.S. Gray, J.D. Hey, D.L. Hillis, J.T. Hogan, L. Konan, R. Leners, A.M. Messian, A. Pospieszczyck, U. Samm, R.P. Schorn, B. Schweer, G. Telesca, R. Vannieuwenhove and P.E Vandenplas, Nucl. Fusion **32**, 837 (1992).
[10] R.R. Weynants, S. Jachmich and G. Van Oost, Plas. Phys. Control Fusion **40**, 635 (1998).

[11] J. Boedo, D. Gray, S. Jachmich, R. Conn, G.P. Terry, G. Tynan, G. Van Oost, R.R. Weynants and TEXTOR Team, Nucl. Fusion **40**, 7 (2000).
[12] J.A. Boedo, D.S. Gray, P.W.Terry, S. Jachmich, G.R. Tynan, R.W. Conn and TEXTOR-94 Team, Nucl. Fusion, **42**, 117 (2002).
[13] B. Friedman, T.A. Carter, M.V. Umansky, D. Schaffner and B. Dudson, Phys. Plasmas **19**, 102307 (2012).
[14] P.W. Terry and R. Gatto, Phys. Plasmas **13**, 062309 (2006).
[15] G.M. Staebler, R.E. Waltz, J.E. Kinsey and W. Solomon in *Proceedings of the 24th Fusion Energy Conference, San Diego, 2012* (International Atomic Energy Agency, Vienna, 2012).
[16] H. Biglari, P.H. Diamond and P.W. Terry, Phys. Fluids B. **2**, 1 (1990).
[17] K.C. Shaing, E.C. Crume and W.A. Houlberg, Phys. Fluids B **2**, 6 (1990).
[18] Y.Z. Zhang and S.M. Mahajan, Phys. Fluids B **4**, 1385 (1992).
[19] Y.Z. Zhang and S.M. Mahajan, Phys. Fluids B **5**, 7 (1993).
[20] A.S. Ware, P.W. Terry, P.H. Diamond and B.A. Carreras, Plasma Phys. Control Fusion **38**, 1343 (1996).
[21] A.S. Ware, P.W. Terry, B.A. Carreras and P.H. Diamond, Phys. Plasmas **5**, 173 (1998).
[22] P.W. Terry, D.E. Newman and A.S. Ware, Phys. Rev. Lett. **87**, 185001 (2001).
[23] E.-J. Kim and P.H. Diamond, Phys. Rev. Lett. **90**, 7 (2003).
[24] E.-J. Kim and P.H. Diamond, Phys. Plasmas **11**, 10 (2004).
[25] M. Leconte, P. Beyer, S. Benkadda and X.Garbet, Phys. Plasmas **13** 112301 (2006).
[26] A.P.L. Newton and E.-J. Kim, Phys. Plasmas **14**, 122306 (2007).
[27] A.P.L. Newton and E.-J. Kim, Phys. Plasmas **18**, 052305 (2011).
[28] W. Gekelman, H. Pfister, Z. Lucky, J. Bamber, D. Leneman and J. Maggs, Rev. Sci. Instrum. **62**, 2875 (1991).